ACS APPLIED MATERIALS & INTERFACES

www.acsami.org

Research Article

Importance of Vacancies and Doping in the Hole-Transporting Nickel Oxide Interface with Halide Perovskites

Boubacar Traore,* Laurent Pedesseau, Jean-Christophe Blancon, Sergei Tretiak, Aditya D. Mohite, Jacky Even, Claudine Katan, and Mikaël Kepenekian*

Cite This: *ACS Appl. Mater. Interfaces* 2020, 12, 6633−6640

Read Online

ACCESS | Metrics & More | Article Recommendations | Supporting Information

ABSTRACT: Nickel oxide (NiO) is a commonly used contact material for a variety of thin-film optoelectronic technologies based on organic or hybrid materials. In such setups, interfaces play a crucial role as they can reduce, if not kill, the device performances by bringing additional traps or energy barriers, hindering the extraction of charge carriers from the active layer. Here, we computationally examine a prototype halide perovskite architecture, NiO/$MAPbI_3$ ($MA = CH_3NH_3^+$), that has shown excellent photovoltaic performance and, in particular, a large open-circuit voltage. We show that efficient hole collection is achieved only when considering the role of vacancies induced by standard material deposition techniques. Specifically, Ni vacancies lead to nearly perfect valence band energy level alignment between the active layer and the contact material. Finally, we show how Li doping greatly improves the performances of the device and further propose alternative dopants. Our results suggest the high tunability of NiO interfaces for the design of optimized optoelectronic devices far beyond that of halide perovskites.

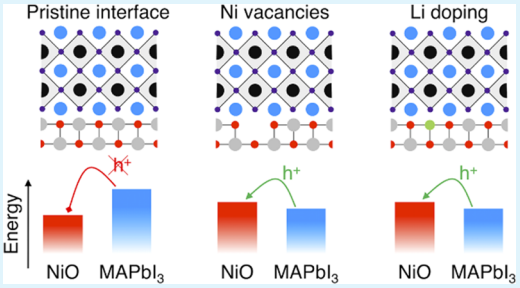

KEYWORDS: *nickel oxide, tuning interface energetics, density functional theory, hole transport, defects and doping*

INTRODUCTION

Tuning interface energetics in thin-film optoelectronic devices is of paramount importance. In such devices, the photoactive material is typically sandwiched between charge collection layers, which are referred to as an electron transport layer (ETL) and a hole transport layer (HTL). Poorly matched and designed interfaces can lead to energy level and dielectric mismatches along with traps causing undesired charge carriers recombination that may overall reduce the performances of the photoactive layer.[1,2] Hence, their selection and optimization play an essential role in the performance of optoelectronic devices.[2−4] Among HTL materials, the inorganic transition-metal oxide, nickel oxide (NiO), is an attractive technological and relatively inexpensive solution including low-cost solution process deposition techniques.[5] Its adoption in photovoltaics was triggered by the pioneering works of He et al.[6] and Irwin et al.[7] in dye-sensitized solar cells (DSSCs) and organic photovoltaic (OPV) devices, respectively. Moreover, NiO finds extensive applications as a transparent conductive oxide[8] in water splitting[9] and batteries.[10] The interest for NiO in these diversified fields takes root from its wide band gap (>3.6 eV), p-type conduction, and magnetic and optical refraction properties.

Recently, some of these features were exploited in the context of hybrid organic−inorganic perovskite (HOP)-based optoelectronic devices. These studies have been motivated by the power conversion efficiency of HOP-based photovoltaics, which nowadays competes with that of silicon solar cells.[11] In particular, HOP solar cells exhibit attractive photovoltaic performances when NiO is used as an HTL in stable large-area architectures or monolithic HOP/silicon tandem devices.[12−16] The improved performance was attributed to the near-ideal valence band energy alignment between NiO and, for instance, methylammonium ($MA = CH_3NH_3^+$) lead iodide, $MAPbI_3$.[17,18] Besides, the experimental measurements point to an increased photovoltaic power conversion efficiency when NiO is doped with Li.[18] A few theoretical works describe the interface of halide perovskites with TiO_2,[19] even fewer deal with other HTL.[20] As a consequence, the fundamental understanding of the origin of such a near-ideal alignment between NiO and $MAPbI_3$ with and without Li doping is lacking.

Here, we study an archetypal interface through first-principles calculations based on density functional theory (DFT) by examining in detail NiO junctions with the prototypical HOP material, $MAPbI_3$. Considering the defect-free interface, we find that the high-frequency dielectric constant profile across the interface presents a low dielectric contrast between the two materials, which benefits hole

Received: October 28, 2019
Accepted: January 9, 2020
Published: January 9, 2020

extraction. However, our results show that the valence band energy level alignment between pristine NiO and $MAPbI_3$ materials is not favorable for hole extraction. In contrast, we show a significant change in the valence band energetics of NiO due to native Ni vacancies appearing in the material deposition. This is consistent with ultraviolet photoelectron spectroscopy (UPS) experiments. Therefore, we demonstrate that the widely accepted view of near-ideal experimental valence band energy level alignment between NiO and $MAPbI_3$ is related to these Ni vacancies. Finally, we show that Li doping improves the level alignment and propose Cs and Rb as alternative dopants of NiO to further tune its interfacial energetics. The methodology developed in this report will be directly transferable to the understanding of other types of interfaces including various perovskites, conventional semiconductors, and alternative carrier transport layer materials.

RESULTS AND DISCUSSION

NiO and $MAPbI_3$ Bulk Materials. NiO is a prototype transition-metal oxide that has been extensively scrutinized over the years.[21−24] The localized Ni 3d electrons make it a highly correlated system, whose theoretical description fails in the local density approximation (LDA) or the generalized gradient approximation (GGA) of DFT.[25] Hence, we adopted the so-called LDA + U (or GGA + U) method[26,27] by applying a Hubbard-like correction term U to Ni 3d orbitals within the SIESTA code (see the Supporting Information, SI).[28,29] In previous works, the method has been successful in describing the magnetic properties of NiO and results in a band gap that is in a fair agreement with the experiment.[26,27] In our case, we found that an effective U value (U_{eff}) of 6.0 eV was well suited to capture the main features of the electronic structure of NiO and was consistently used across different calculations for comparison. We note that this value falls within the accepted range of appropriate U values reported for NiO in the literature.[27,30] The detailed description of the electronic structure of NiO and the selection of U_{eff} can be found in the SI (Text S1). Briefly, the electronic band gap of NiO corresponds to a charge-transfer-type excitation (Text S2, SI) and the calculated magnetic moment of Ni (1.77 μ_B) is in excellent agreement with the experimental value (~1.7 μ_B).[31] Moreover, the computed relaxed lattice constant (a = 4.25 Å) presents less than 2% error as compared to the experimental structure (a = 4.167 Å).[32]

The $MAPbI_3$ perovskite and its alloys, involving formamidinium cations and mixed cations/halides, have so far produced the most efficient solar cells.[33,34] Structurally, $MAPbI_3$ forms a three-dimensional lattice where corner-shared PbI_6^{2-} octahedra extend in all directions with MA cation tumbling around the center of the cubo-octahedra. Over the past years, impressive chemical and materials engineering of HOP has been carried out not only to increase their efficiencies but also to improve their stabilities and photophysical properties.[2,16] Here, we use its orthorhombic phase with well-defined positions of MA to avoid the issue of the dynamical disorder of the latter in the tetragonal and cubic structures.[35] This low-temperature phase has been extensively studied, and DFT-based calculations provide a correct description of the main electronic features, in particular, the direct band gap at Γ point (Figure S2, SI). Let us note that, because of the presence of the heavy atom Pb, the correct treatment of $MAPbI_3$ should include spin−orbit coupling (SOC). However, the impact of SOC on valence band states is negligible (Figure S2, SI); thus, it is reasonable to neglect SOC in our DFT calculations focusing on the NiO/$MAPbI_3$ interface for hole extraction only (spin polarization, however, is included).

NiO/$MAPbI_3$ Pristine Interface. Considering the experimentally observed (100) surface of NiO and corresponding lattice parameters,[31,32] the $MAPbI_3$(010) surface affords appropriate lattice matching for a NiO/$MAPbI_3$ interface (Table S3, SI). The resulting lateral lattice mismatch between $MAPbI_3$ and NiO is less than 3%. Details related to the interface construction can be found in Text S3 (SI).

To combine NiO and $MAPbI_3$ at the interface, we terminated $MAPbI_3$ by MAI (Figure 1a) as suggested by STM measurements[36] and reported to be the favorable termination using DFT.[37] The interface relaxes such that iodine atoms point toward nickel atoms (Figure 1b) with a Ni−I bond length of about 2.87 Å, in good agreement with the bulk Ni−I bond distance of 2.78 Å in hexagonal $R\bar{3}m$ NiI_2.[38] The resulting band structure (Figure 1c) shows a direct band gap at Γ point. The wavefunction plot of the valence band maximum (VBM) at Γ point reveals an antibonding hybridization between Pb(6s)−I(5p) states only (Figure 1d), whereas the same band shows NiO states at the in-plane M_{xy} point. Stated differently, hole wavefunctions are localized inside the perovskite at Γ point, while they are delocalized between both the perovskite and NiO at M_{xy} point. The presence of I states at M_{xy} point is consistent with Ni−I bond formation and shows an efficient coupling between $MAPbI_3$ and NiO.

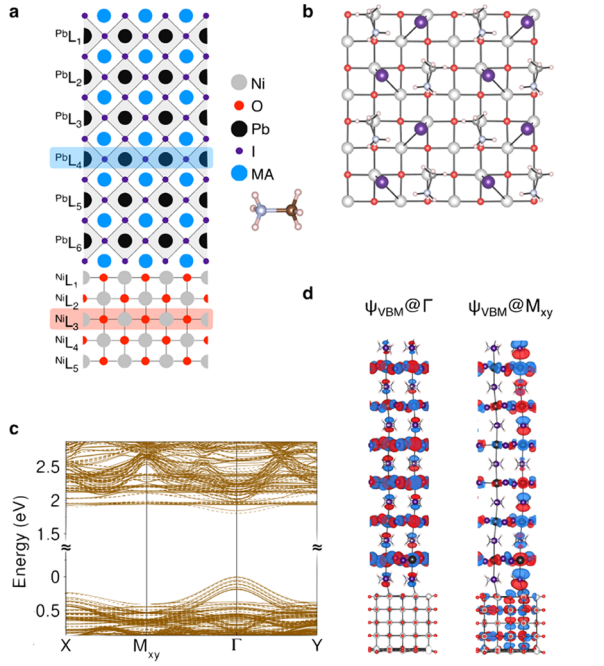

Figure 1. Lattice structure and electronic properties of the NiO/$MAPbI_3$ interface. (a) Model used in our calculations and layer labels. (b) Favorable iodine positions at the interface with I atoms pointing toward Ni in a bridgelike configuration. Here, I, Ni, O, N, C, and H atoms are depicted in purple, light gray, red, blue, dark gray, and pale pink, respectively. (c) Band structure of the relaxed interface model with a direct band gap at Γ point. The valence band maximum (VBM) at Γ point is taken as the energy reference. Plain and dashed lines correspond to majority and minority spins, respectively. (d) VBM wavefunction at Γ and M_{xy} points. Hybridized $MAPbI_3$ and NiO states appear at M_{xy} point, while $MAPbI_3$ dominates at Γ point.

https://dx.doi.org/10.1021/acsami.9b19457
ACS Appl. Mater. Interfaces 2020, 12, 6633−6640

Efficient charge separation in solar cell devices, and, more generally, semiconductor heterostructures, depends on the dielectric properties of the respective materials. If the paired media have different dielectric constants, charge separation through the interface and the subsequent carrier transport may be improved or frustrated depending on the extent of the dielectric mismatch.[1] In our NiO/$MAPbI_3$ interface, we evaluated the dielectric constants by considering the high-frequency component (ϵ_∞) along the interface direction using a first-principles-based approach described elsewhere.[39,40] Figure 2 shows the profile of ϵ_∞ along the interface through NiO and

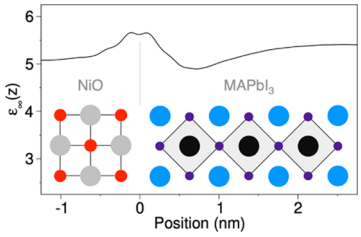

Figure 2. High-frequency dielectric constant profile of the NiO/$MAPbI_3$ interface. The dielectric mismatch is low, which points to efficient charge extraction at the interface. The inset shows the corresponding position of the NiO/$MAPbI_3$ slab.

$MAPbI_3$ layers. In their central bulklike regions, both NiO (ϵ_∞ = 5.1) and $MAPbI_3$ (ϵ_∞ = 5.4) have values that are comparable to those calculated for their bulk experimental structures (Figure S4, SI). The calculated values for NiO and $MAPbI_3$ are also in a good agreement with the experimentally measured values amounting to 5.7 and 6.5, respectively.[41,42] At the interface region, the dielectric constant shows a local peak, which is, to some extent, related to the NiO interface states that hybridize with those of $MAPbI_3$, resulting in an interface dipole that we estimated to be about 2.0 debye. Interestingly, the two dielectric constants (ϵ_∞) are comparable, indicative of a low dielectric contrast/mismatch between $MAPbI_3$ and NiO. This may hint to an efficient charge separation across the interface due to the possible reduced binding energy of holes as a result of low dielectric mismatch.[1] It is worth noting that, in the actual room temperature solar cell operation, low-frequency static dielectric constant (ϵ_s) also plays an important role and may represent a dominant contribution in the response of charge carriers to the electric field.[43] Effective ϵ_s values ranging from 11 to 20 can be expected in $MAPbI_3$ due to optical phonons and rotational tumbling of organic cations,[43,44] whereas this value amounts to 11.90 for NiO.[41]

For an efficient hole transmission from the perovskite layer to the hole transport material, the VBM of the latter should be above that of the former. A parameter that quantifies the shift between the VBM of the heterostructure materials is referred to as the valence band offset (VBO). Here, it is defined as the difference between VBM_{NiO} and VBM_{MAPbI_3} from their bulklike layers.[45] Therefore, positive values for VBO indicate that NiO states stand higher in energy than the respective $MAPbI_3$ states, an ideal situation for hole extraction. In contrast, negative values lead to an unfavorable interface for solar cell applications. Our calculations imply the presence of $MAPbI_3$ states above those of NiO (Figure 1c), pointing to a valence band energy level alignment that is detrimental for hole collection. This is confirmed by a layer-resolved projected density of states (PDOS, Figure 3a). Indeed, from the PDOS, one can extract

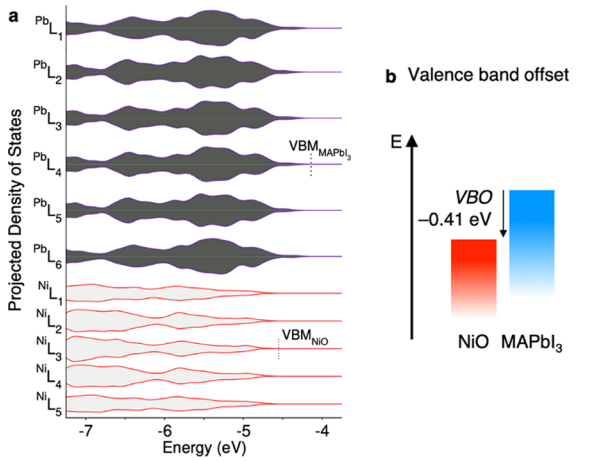

Figure 3. Valence band alignment in the NiO/$MAPbI_3$ pristine interface. (a) Layer-by-layer projected density of states (PDOS) of the relaxed interface model affording valence band alignment from the bulklike parts of $MAPbI_3$ and NiO. (b) Valence band offset (VBO) determined from the PDOS. The computed VBO is not favorable for hole extraction.

the position of the VBM of the layers emulating the bulk of both materials ($^{Ni}L_3$ for NiO and $^{Pb}L_4$ for $MAPbI_3$, Figure 1a). In the case of the $MAPbI_3$/NiO interface, from the PDOS, we obtain a VBO of about −0.41 eV between $MAPbI_3$ and NiO (Figure 3). We obtain a similar VBO (−0.36 eV) using the Hartree potential alignment[46] (Text S4 and Figure S5, SI), showing that both the PDOS and the Hartree potential alignment methods can be used to compute band offsets.[45,47] Surprisingly, the sign of our calculated VBO value seemingly contradicts the experimental findings, which point to an almost ideal VBO (ranging from +0.0 to +0.4 eV) between $MAPbI_3$ and NiO, making the latter a suitable material for hole extraction and transport.[14,18,48,49]

Since this finding contrasts with experimental results, we checked that it was neither an artifact of the choice of the starting orthorhombic structure nor the considered number of layers in $MAPbI_3$ or our computational approach. First, we obtained similar results with tetragonal $MAPbI_3$ as the starting structure of the interface (Text S5 and Figure S6, SI) and by increasing the number of layers in both $MAPbI_3$ and NiO (Text S6 and Figure S7, SI). Then, we recalculated the electronic structure using the GGA + *U* formalism in planewave basis sets instead of localized basis sets (Text S7, SI). These new simulations lead to a negative VBO of −0.53 eV, confirming the counterintuitive result. Hybrid functional calculations (HSE03[50] and HSE06[51]) also confirm the trend (VBO ≈ −0.70 eV). Thus, the sign of VBO is not an artifact of the Hubbard correction approach (Text S8, SI).

While the DFT approach is not responsible for the sign of the VBO, it might be influenced by the structural choices made in the construction of the NiO/$MAPbI_3$ interface. Indeed, despite that STM experiments point to an MAI termination in $MAPbI_3$,[36] PbI_2 termination may not be completely excluded as it is reported to be slightly more stable by other first-principles simulations.[52,53] To assess the possible effect of this termination on the electronic structure of the NiO/$MAPbI_3$ interface model, we considered the same interface but with PbI_2 termination (Text S9 and Figure S11, SI). We find that the most stable configuration presents a VBO shift of −0.15 eV with $MAPbI_3$ states above those of NiO, indicative of an

https://dx.doi.org/10.1021/acsami.9b19457
ACS Appl. Mater. Interfaces 2020, 12, 6633−6640

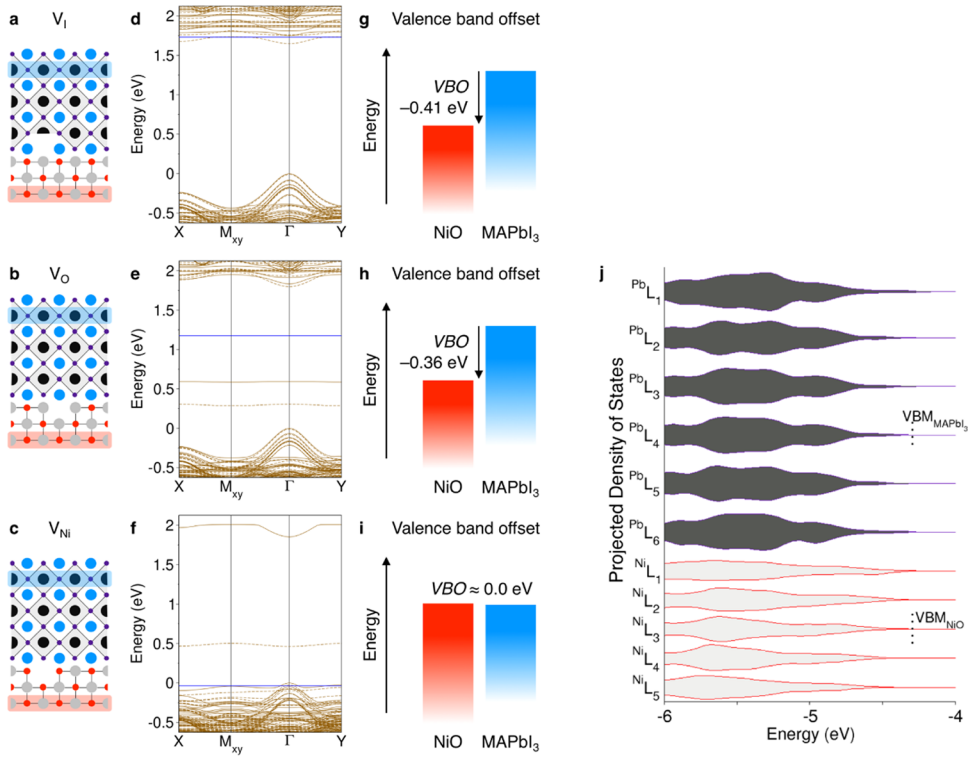

Figure 4. Role of vacancies in the NiO/$MAPbI_3$ interface. (a–c) Iodine (V_I), oxygen (V_O), and nickel (V_{Ni}) vacancy models, respectively. (d–f) Corresponding calculated band structures. The valence band maximum at the Γ point is taken as the energy reference; a blue line marks the Fermi level. Plain and dashed lines correspond to majority and minority spins, respectively. (g–i) Corresponding computed valence band offsets. (j) Layer-by-layer projected density of states (PDOS) of the interface model with V_{Ni} resulting in the VBO shown in (i). Nickel vacancies produce a valence band alignment favorable to hole extraction.

unfavorable alignment for hole collection. We note that, in real thin films, several interface configurations may coexist depending on the deposition technique and conditions. This could eventually lead to the formation of some metastable domains in the device, thus affecting the interfacial energetics (Figure S12, SI). However, we hypothesize that the thermodynamics of the system should make the favorable energy configurations to dominate.

Finally, considering the effect of substituting the cation in the perovskite layer, we also inspected the energy level alignment of the $FAPbI_3$/NiO interface (Text S10, SI) with FA referring to formamidinium (FA = $CH(NH_2)_2$). Here, we used the (001) surface of cubic $FAPbI_3$ with FAI termination and lattice-matched it to NiO, the latter being the substrate. We calculated a VBO of −0.15 eV with $FAPbI_3$ states above those of NiO (Figure S13, SI). As in $MAPbI_3$, this VBO is not optimal for hole collection from $FAPbI_3$ to NiO. However, the absolute value of this shift is lower as compared to −0.41 eV obtained with $MAPbI_3$. Detailed information on this interface, the related discussion on the lower VBO with $FAPbI_3$, and possible effects of mixed-cation HOP on the properties of this interface can be found in Text S10 (SI). In the end, all of these results confirm a valence band energy level alignment that is not in favor of efficient hole collection when considering defect-free interfaces of pristine materials.

Hence, a legitimate question about the possible origin of this apparent contradiction arises. Could it be related to the assumption of the defect-free NiO and $MAPbI_3$ lattices in our model? What is the role of doping in the experimentally reported VBO? In the following, we aim to address these questions.

Role of Vacancies. Despite hybrid perovskites being referred to as "defect-tolerant",[54−56] various defects are abundant in these materials and their role in the interfacial properties of $MAPbI_3$ remains elusive. While it is of great fundamental and technological interest, there is no theoretical study of their effects on the electronic structure of the NiO/$MAPbI_3$ interface, which we address in this section. To introduce defects and later dopants into the interface model, we enlarge the defect-free cell to reduce the effects of spurious interactions, originating from the periodic boundary conditions, on the computed properties (see Text S11, SI). We consider the impact of different defects that could potentially influence the valence band alignment: iodine vacancies (V_I, Figure 4a), oxygen vacancies (V_O, Figure 4b), and nickel vacancies (V_{Ni}, Figure 4c). Furthermore, MA vacancies (V_{MA}), Pb vacancies (V_{Pb}), and Schottky-type defect MAI vacancies (V_{MAI}) are presented in the SI (Text S11, SI).

The band structure of V_I (Figure 4d) shows a shallow defect level at the conduction band, in agreement with previous results,[57] while having a negligible effect on the valence band. In the case of V_O, localized midgap trap states are formed. The analysis of the wavefunctions shows that these states arise from Ni atoms in direct contact with the vacant oxygen site. Such midgap states are a source of nonradiative recombinations detrimental to photovoltaic performances. However, similar to V_I, the presence of V_O brings no change to the shape of the valence bands. Both V_I and V_O barely affect the VBO of the interface model as compared to the defect-free cell, and we obtain a negative value of ca. −0.40 eV for the two systems (Figure 4g,h).

https://dx.doi.org/10.1021/acsami.9b19457
ACS Appl. Mater. Interfaces 2020, 12, 6633−6640

Similarly, we calculate a VBO of ca. −0.31 eV for V_{MAI} with the valence band barely affected (Figure S15, SI). V_{MA} and V_{Pb} at the interface region ($^{Pb}L_6$) present VBO values of −0.05 and −0.10 eV, respectively, and the Fermi level is shifted to the valence bands, forming shallow acceptor states, in agreement with previous reports (Figures S16−S19, SI).[58,59] In the bulklike region of $MAPbI_3$ ($^{Pb}L_4$), VBO values of V_{MA} and V_{Pb} become ca. −0.46 and −0.41 eV, respectively (Figures S17 and S19, SI). Hence, with $MAPbI_3$-related defects along with V_O, VBO remains essentially unfavorable for hole collection across the NiO/$MAPbI_3$ interface.

On the other hand, the presence of a V_{Ni} site at both the interface and bulklike layers ($^{Ni}L_1$ and $^{Ni}L_3$) is accompanied by the emergence of less dispersive bands (Figure 4f and Figure S20, SI) that are localized on O atoms (2p states) around V_{Ni} and the next-neighboring Ni atoms (3d states). It is worth noting that it results in a large positive energy shift of the valence bands related to NiO, which becomes almost equal to the VBM of the $MAPbI_3$ (Figure 4f and Figures S20−S22, SI). As a consequence, the VBO becomes almost vanishing (Figure 4i,j) and the material system becomes p-type (Fermi energy crosses the valence states). The latter result is in agreement with the valence band alignments given in the literature between $MAPbI_3$ and NiO.[14,49] It is known that V_{Ni} turns NiO to a p-type semiconductor,[60,61] but its effect on the interfacial properties of $MAPbI_3$ has not been assessed previously. This is an important point: It indicates that the presence of V_{Ni} in NiO with $MAPbI_3$ is probably at the origin of the measured near-ideal energy alignment between the two materials. This is plausible considering the standard fabrication processes (sputtering, spin-coating, etc.) of NiO as this oxide is experimentally known to be generally Ni-deficient.[62]

Experimental Confirmation. The reported experimental energy level alignments between NiO and $MAPbI_3$ generally, if not all, rely on the difference between the work functions (W_F) of NiO and the absolute valence band energy (AVBE) of $MAPbI_3$. While the AVBE of ca. −5.4 eV for $MAPbI_3$ seems more consensual in the realm of reported data,[63] the measured W_F for NiO largely depends on the processing conditions and NiO surface exposure.[64] The reported W_F values fall between −5.0 and −5.6 eV,[5,7,64−66] reaching as high as −6.2 to −6.7 eV in pure NiO film deposited in situ.[64] For a purely processed NiO film, its W_F can be assumed to be close in value to its AVBE as its purity makes it stoichiometric with no defect. Indeed, the measured UPS absolute valence band energy of −6.5 eV[67,68] for NiO agrees well with the W_F of purely deposited NiO. Hence, using an AVBE of −6.2 to −6.5 eV for NiO to align it with $MAPbI_3$, the resulting VBO gives −0.8 to −1.1 eV, which is in good agreement with our prediction for the defect-free NiO/$MAPbI_3$ interface model (Figure 3b). Moreover, considering W_F of NiO in air-exposed conditions (ca. −5.4 eV), with potential defects like Ni vacancies,[62] we recover the literature-reported near-ideal valence band alignment between NiO and $MAPbI_3$. This is in a good agreement with our predictions on the role of Ni vacancies in turning NiO into a p-type material in the interface model. Therefore, we believe that the experimentally reported deposited NiO films via sputtering/spin-coating during HOP fabrication present dominant Ni vacancies,[62] which appear to help the performances of nickel-based perovskite solar cells. However, the appearance of the less dispersive midgap defectlike states due to the presence of V_{Ni} at the interface can alleviate the efficiency of hole carrier collection at the NiO/$MAPbI_3$ interface. Since all of the investigated defects, except V_{Ni}, lead to a negative VBO, we postulate that increasing their concentration would only worsen the properties of this interface. Therefore, it is desirable to limit and/or reduce their concentration inside the film while, at the same time, preserving an ideal energy alignment. A practical strategy to achieve that goal is by doping, which is discussed in the next section.

Role of Doping. Similar to other semiconductors, doping strategies have been used to fine-tune the properties of NiO, notably using Li for improved p-conductivity[69,70] and solar efficiencies in perovskites.[18,71] To bring more fundamental understanding to this improvement, we study the effect of Li doping of NiO by considering the substitution in our simulation cell of two Ni atoms, chosen as far from each other as possible, by two Li atoms (Figure 5a). The doping is done at the interface region of NiO ($^{Ni}L_1$, Figure 5b) in direct contact with $MAPbI_3$ and in the bulklike region of NiO ($^{Ni}L_3$, Figure 1c). Li doping at the interface-like region is 1.5 eV (0.75 eV per Li atom) more favorable than in the bulklike region. Hence, our results indicate that the doped Li atoms would probably be distributed in NiO at the interface region being in contact with $MAPbI_3$. Nevertheless, the other configurations cannot be completely excluded given the relatively low energy difference for the system size modeled.

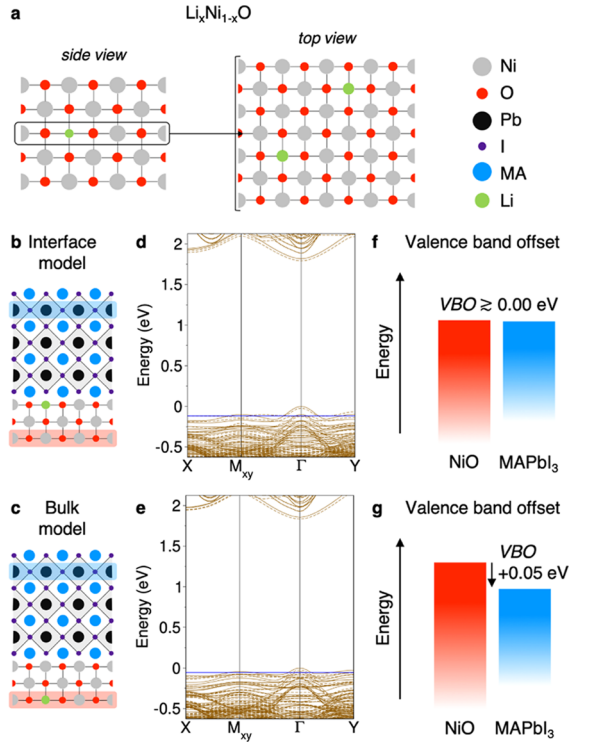

Figure 5. Role of Li doping in the NiO/$MAPbI_3$ interface. (a) $Li_xNi_{1-x}O$ models with dopants spread across a NiO layer. (b) Interface model where the doped layer is at the interface. (c) Bulk model where the dopants are placed in the bulklike layer. Calculated band structures of (d) interface and (e) bulk models. The valence band maximum at the Γ point is taken as the energy reference;, a blue line marks the Fermi level. Plain and dashed lines correspond to majority and minority spins, respectively. (f, g) Corresponding computed valence band offsets. Both situations lead to a favorable hole extraction.

The band structures of "Li at the interface" (Figure 5d) and "Li in the bulk" (Figure 5e) regions show that Li doping facilitates a p-type conduction, while no localized band is

https://dx.doi.org/10.1021/acsami.9b19457
ACS Appl. Mater. Interfaces 2020, 12, 6633−6640

created in the gap. The reorganization of the valence bands under the influence of Li, as shown by the PDOS (Figures S23 and S24, SI), leads to an improved VBO value that becomes slightly positive (+0.00 eV for Li at the interface region and +0.05 eV at the bulk one, Figure 5f,g). Therefore, Li doping recovers an ideal valence energy alignment obtained with V_{Ni} while suppressing the presence of nondispersive midgap states. Since dopants are not always evenly distributed in the materials, we also consider a model in which the two substituted Ni atoms are only separated by one O atom (Figures S23 and S24, SI). This configuration could be viewed as a well-controlled NiO-doped system with a high concentration of Li in a confined region of the material. Energetically, the original spread model is 0.3 eV (0.15 eV per Li atom), more favorable than the clustered one at both the interface-like and bulklike regions. We notice that the VBO shift increases when Li atoms are clustered in a confined space, resulting in +0.31 and +0.26 eV values at the interface-like and bulklike regions, respectively. We also examined the effect of increased dopant concentration by substituting four Ni atoms by Li atoms, bringing the concentration to 5%. Again, we examined configurations where Li atoms are clustered in one layer and spread across two NiO layers (Figure S25, SI). Here, VBO varies from +0.21 eV when Li atoms are "clustered" to +0.15 eV when they are spread (Figure S25, SI). This suggests that 5% of Li content in NiO should improve the conversion efficiency of the HOP device as a result of increased open-circuit voltage.

The calculated improved energy level alignment of Li-doped NiO with $MAPbI_3$ is in agreement with the enhanced efficiency of $LiNiO_x/MAPbI_3$ devices as compared to that of undoped NiO.[18,71] The PDOS of the different systems with Li doping shows that the introduction of Li pushes NiO states to the same energy level or above those of $MAPbI_3$ while reinforcing their hybridization at the valence band maximum (Figures S26, SI). At the same time, Li states remain about 0.5 eV below (Figure S26, SI). The net effect results in a doped NiO being a better hole transport layer.

Interestingly, we obtained an increased VBO ($\geq$0.00 eV) of the $NiO/MAPbI_3$ heterostructure when NiO is doped with Rb and Cs atoms (Figures S27 and S28, SI). As with Li, their insertion into NiO enhances the hybridization between $MAPbI_3$ and the HTL. With Rb doping, we calculated a VBO of +0.46 eV (Figure S27, SI). For Cs, we calculated a VBO of +0.41 eV (Figure S28, SI). The large atomic size of Rb and Cs induces more structural relaxation at the interface, causing an increase of VBO. Given that Cs and Rb are already adopted as cations in mixed-cation 3D HOP,[16,33] they may be considered as alternative dopants of NiO in the search for optimizing the efficiency of $MAPbI_3$ solar devices.

CONCLUSIONS

In summary, we demonstrate the role of native defects and doping in the energetics and charge carrier extraction for devices based on NiO interfaces. Our computed valence band offsets are consistent with experimental UPS absolute valence band energies of NiO. Moreover, our analysis clarifies the experimentally reported ideal valence band alignment between $MAPbI_3$ and NiO, which is related to the intrinsic Ni vacancies of the hole-transporting material. The appearance of these dominant Ni vacancies commensurates with an experimental report on standard NiO processing conditions.[62] Furthermore, we highlight the effect of Li doping on NiO to reach improved energy alignment of the perovskite–NiO interface, fostering enhanced hole extraction. Hence, we propose alternatives to Li doping of NiO such as Cs or Rb to further fine-tune the NiO interfacial energetics. Additionally, we highlight the importance of the dielectric mismatch. For instance, the dielectric properties related to the high-frequency component of the interface indicate a low dielectric mismatch between $MAPbI_3$ and NiO, which benefits hole collection. The combined results bring together a holistic picture of the interfacial properties of NiO. Our findings open avenues for the optimization of thin-film devices based on NiO contacts and help the reader to adopt relevant theoretical strategies to model the properties of heterostructures.

ASSOCIATED CONTENT

Supporting Information

The Supporting Information is available free of charge at https://pubs.acs.org/doi/10.1021/acsami.9b19457.

Computational details, electronic structure of NiO, detailed description of the construction of the interface models, energy level alignment using Hartree potential profiles, additional planewave calculations on valence band energy level alignments, effects of $MAPbI_3$ surface termination and substituting MA cation on the valence band offset of $MAPbI_3$/NiO, projected density of states for systems with vacancies or dopants, and band structures for systems with dopants (PDF)

AUTHOR INFORMATION

Corresponding Authors

Boubacar Traore − *Univ Rennes, INSA Rennes, CNRS, Institut FOTON − UMR 6082, Rennes F-35000, France; Univ Rennes, ENSCR, CNRS, ISCR − UMR 6226, Rennes F-35000, France;* orcid.org/0000-0003-0568-4141;
Email: boubacar.traore@insa-rennes.fr

Mikaël Kepenekian − *Univ Rennes, ENSCR, CNRS, ISCR − UMR 6226, Rennes F-35000, France;*
Email: mikael.kepenekian@univ-rennes1.fr

Authors

Laurent Pedesseau − *Univ Rennes, INSA Rennes, CNRS, Institut FOTON − UMR 6082, Rennes F-35000, France;* orcid.org/0000-0001-9414-8644

Jean-Christophe Blancon − *Department of Chemical and Biomolecular Engineering, Rice University, Houston, Texas 77005, United States*

Sergei Tretiak − *Los Alamos National Laboratory, Los Alamos, New Mexico 87545, United States;* orcid.org/0000-0001-5547-3647

Aditya D. Mohite − *Department of Chemical and Biomolecular Engineering, Rice University, Houston, Texas 77005, United States;* orcid.org/0000-0001-8865-409X

Jacky Even − *Univ Rennes, INSA Rennes, CNRS, Institut FOTON − UMR 6082, Rennes F-35000, France;* orcid.org/0000-0002-4607-3390

Claudine Katan − *Univ Rennes, ENSCR, CNRS, ISCR − UMR 6226, Rennes F-35000, France;* orcid.org/0000-0002-2017-5823

Complete contact information is available at: https://pubs.acs.org/10.1021/acsami.9b19457

Notes

The authors declare no competing financial interest.

https://dx.doi.org/10.1021/acsami.9b19457
ACS Appl. Mater. Interfaces 2020, 12, 6633−6640

■ ACKNOWLEDGMENTS

ISCR and FOTON have received funding from the European Union's Horizon 2020 program, through a FET Open Research and Innovation Action under the Grant agreement no. 687008. The work at the Institut des Sciences Chimiques de Rennes was supported by Agence Nationale pour la Recherche (TRANS-HYPERO project). J.E. acknowledges financial support from the Institute Universitaire de France. This work was performed, in part, at the Center for Integrated Nanotechnologies, a US Department of Energy, Office of Science User Facility. S.T. acknowledges support from the LANL LDRD program. This work was granted access to the HPC resources of [TGCC/CINES/IDRIS] under the allocations 2016-x2016097682/2017-A0010907682/2018-A0010907682 made by GENCI.

■ REFERENCES

(1) Sherkar, T. S.; Koster, L. J. A. Dielectric Effects at Organic/Inorganic Interfaces in Nanostructured Devices. *ACS Appl. Mater. Interfaces* **2015**, *7*, 11881−11889.
(2) Schulz, P.; Cahen, D.; Kahn, A. Halide Perovskites: Is It All about the Interfaces. *Chem. Rev.* **2019**, *119*, 3349−3417.
(3) Chueh, C.-C.; Li, C.-Z.; Jen, A. K.-Y. Recent Progress and Perspective in Solution-Processed Interfacial Materials for Efficient and Stable Polymer and Organometal Perovskite Solar Cells. *Energy Environ. Sci.* **2015**, *8*, 1160−1189.
(4) Yip, H.-L.; Jen, A. K.-Y. Recent Advances in Solution-Processed Interfacial Materials For Efficient And Stable Polymer Solar Cells. *Energy Environ. Sci.* **2012**, *5*, 5994−6011.
(5) Steirer, K. X.; Chesin, J. P.; Widjonarko, N. E.; Berry, J. J.; Miedaner, A.; Ginley, D. S.; Olson, D. C. Solution Deposited NiO Thin-Films As Hole Transport Layers in Organic Photovoltaics. *Org. Electron.* **2010**, *11*, 1414−1418.
(6) He, J.; Lindström, H.; Hagfeldt, A.; Lindquist, S.-E. Dye-Sensitized Nanostructured Tandem Cell-First Demonstrated Cell With a Dye-Sensitized Photocathode. *Sol. Energy Mater. Sol. Cells* **2000**, *62*, 265−273.
(7) Irwin, M. D.; Buchholz, D. B.; Hains, A. W.; Chang, R. P. H.; Marks, T. J. p-Type Semiconducting Nickel Oxide As An Efficiency-Enhancing Anode Interfacial Layer In Polymer Bulk-Heterojunction Solar Cells. *Proc. Natl. Acad. Sci. USA* **2008**, *105*, 2783−2787.
(8) Sato, H.; Minami, T.; Takata, S.; Yamada, T. Transparent Conducting p-Type NiO Thin Films Prepared By Magnetron Sputtering. *Thin Solid Films* **1993**, *236*, 27−31.
(9) Kato, H.; Asakura, K.; Kudo, A. Highly Efficient Water Splitting into H_2 and O_2 over Lanthanum-Doped $NaTaO_3$ Photocatalysts with High Crystallinity and Surface Nanostructure. *J. Am. Chem. Soc.* **2003**, *125*, 3082−3089.
(10) Varghese, B.; Reddy, M. V.; Yanwu, Z.; Lit, C. S.; Hoong, T. C.; Subba Rao, G. V.; Chowdari, B. V. R.; Wee, A. T. S.; Lim, C. T.; Sow, C.-H. Fabrication of NiO Nanowall Electrodes for High Performance Lithium Ion Battery. *Chem. Mater.* **2008**, *20*, 3360−3367.
(11) https://www.nrel.gov/pv/cell-efficiency.html (accessed Oct 15, 2019).
(12) You, J.; Meng, L.; Song, T.-B.; Guo, T.-F.; Yang, Y. M.; Chang, W.-H.; Hong, Z.; Chen, H.; Zhou, H.; Chen, Q.; Liu, Y.; De Marco, N.; Yang, Y. Improved Air Stability of Perovskite Solar Cells Via Solution-Processed Metal Oxide Transport Layers. *Nat. Nanotechnol.* **2016**, *11*, 75−81.
(13) Chen, W.; Wu, Y.; Yue, Y.; Liu, J.; Zhang, W.; Yang, X.; Chen, H.; Bi, E.; Ashraful, I.; Grätzel, M.; Han, L. Efficient and Stable Large-Area Perovskite Solar Cells with Inorganic Charge Extraction Layers. *Science* **2015**, *350*, 944−948.
(14) Seo, S.; Park, I. J.; Kim, M.; Lee, S.; Bae, C.; Jung, H. S.; Park, N.-G.; Kim, J. Y.; Shin, H. An Ultra-Thin, Un-Doped NiO Hole Transporting Layer of Highly Efficient (16.4%) Organic-Inorganic Hybrid Perovskite Solar Cells. *Nanoscale* **2016**, *8*, 11403−11412.
(15) Bush, K. A.; et al. 23.6%-Efficient Monolithic Perovskite/Silicon Tandem Solar Cells with Improved Stability. *Nat. Energy* **2017**, *2*, No. 17009.
(16) Tsai, H.; Asadpour, R.; Blancon, J.-C.; Stoumpos, C. C.; Durand, O.; Strzalka, J. W.; Chen, B.; Verduzco, R.; Ajayan, P. M.; Tretiak, S.; Even, J.; Alam, M. A.; Kanatzidis, M. G.; Nie, W.; Mohite, A. D. Light-Induced Lattice Expansion leads to High-Efficiency Perovskite Solar Cells. *Science* **2018**, *360*, 67−70.
(17) Chen, W.; Wu, Y.; Liu, J.; Qin, C.; Yang, X.; Islam, A.; Cheng, Y.-B.; Han, L. Hybrid Interfacial Layer Leads To Solid Performance Improvement of Inverted Perovskite Solar Cells. *Energy Environ. Sci.* **2015**, *8*, 629−640.
(18) Nie, W.; Tsai, H.; Blancon, J.-C.; Liu, F.; Stoumpos, C. C.; Traore, B.; Kepenekian, M.; Durand, O.; Katan, C.; Tretiak, S.; Crochet, J.; Ajayan, P. M.; Kanatzidis, M.; Even, J.; Mohite, A. D. Critical Role of Interface and Crystallinity on the Performance and Photostability of Perovskite Solar Cell on Nickel Oxide. *Adv. Mater.* **2018**, *30*, No. 1703879.
(19) Mosconi, E.; Ronca, E.; De Angelis, F. First-Principles Investigation of the TiO_2/Organohalide Perovskites Interface: The Role of Interfacial Chlorine. *J. Phys. Chem. Lett.* **2014**, *5*, 2619−2625.
(20) Li, L.; Mi, J.; Yong, Y.; Mao, B.; Shi, W. First-Principles Study On the Lattice Plane And Termination Dependence of the Electronic Properties of the NiO/$CH_3NH_3PbI_3$ Interfaces. *J. Mater. Chem. C* **2018**, *6*, 8226−8233.
(21) Du Plessis, P. d. V.; van Tonder, S. J.; Alberts, L. Elastic Constants of a NiO Single Crystal: I. *J. Phys. C: Solid State Phys.* **1971**, *4*, 1983−1987.
(22) Li, J.-L.; Rignanese, G.-M.; Louie, S. G. Quasiparticle Energy Bands of NiO in the GW Approximation. *Phys. Rev. B* **2005**, *71*, No. 193102.
(23) Jiang, H.; Gomez-Abal, R. I.; Rinke, P.; Scheffler, M. First-Principles Modeling of Localized d States with the GW/LDA+U Approach. *Phys. Rev. B* **2010**, *82*, No. 045108.
(24) Panda, S. K.; et al. High Photon Energy Spectroscopy of NiO: Experiment and Theory. *Phys. Rev. B* **2016**, *93*, No. 235138.
(25) Rohrbach, A.; Hafner, J.; Kresse, G. Molecular Adsorption on the Surface of Strongly Correlated Transition-Metal Oxides: A Case Study For CO/NiO(100). *Phys. Rev. B* **2004**, *69*, No. 075413.
(26) Anisimov, V. I.; Aryasetiawan, F.; Lichtenstein, A. I. First-Principles Calculations of the Electronic Structure And Spectra of Strongly Correlated Systems: the LDA+U Method. *J. Phys.: Condens. Matter* **1997**, *9*, 767−808.
(27) Dudarev, S. L.; Botton, G. A.; Savrasov, S. Y.; Humphreys, C. J.; Sutton, A. P. Electron-Energy-Loss Spectra And the Structural Stability of Nickel Oxide: An LSDA+U Study. *Phys. Rev. B* **1998**, *57*, 1505−1509.
(28) Soler, M.; Artacho, E.; Gale, J. D.; Garc, A.; Junquera, J.; Ordejon, P.; Daniel, S. The SIESTA Method for Ab Initio Order-N Materials. *J. Phys.: Condens. Matter* **2002**, *14*, 2745−2779.
(29) Artacho, E.; Anglada, E.; Diéguez, O.; Gale, J. D.; García, A.; Junquera, J.; Martin, R. M.; Ordejón, P.; Pruneda, J. M.; Sánchez-Portal, D.; Soler, J. M. The SIESTA Method; Developments and Applicability. *J. Phys.: Condens. Matter* **2008**, *20*, No. 064208.
(30) Cococcioni, M.; de Gironcoli, S. Linear Response Approach to the Calculation of the Effective Interaction Parameters in the LDA+U Method. *Phys. Rev. B* **2005**, *71*, No. 035105.
(31) Ködderitzsch, D.; Hergert, W.; Temmerman, W. M.; Szotek, Z.; Ernst, A.; Winter, H. Exchange Interactions in NiO and at the NiO(100) Surface. *Phys. Rev. B* **2002**, *66*, No. 064434.
(32) Welton-Cook, M. R.; Prutton, M. LEED Calculations for the NiO (100) Surface: Extension to Lower Energies. *J. Phys. C: Solid State Phys.*. **1980**, *13*, 3993−3400.
(33) Saliba, M.; Matsui, T.; Domanski, K.; Seo, J.-Y.; Ummadisingu, A.; Zakeeruddin, S. M.; Correa-Baena, J.-P.; Tress, W. R.; Abate, A.; Hagfeldt, A.; Grätzel, M. Incorporation of Rubidium Cations Into Perovskite Solar Cells Improves Photovoltaic Performance. *Science* **2016**, *354*, 206−209.

https://dx.doi.org/10.1021/acsami.9b19457
ACS Appl. Mater. Interfaces 2020, 12, 6633−6640

(34) Yang, W. S.; Park, B.-W.; Jung, E. H.; Jeon, N. J.; Kim, Y. C.; Lee, D. U.; Shin, S. S.; Seo, J.; Kim, E. K.; Noh, J. H.; Seok, S. I. Iodide Management in Formamidinium-Lead-Halide-Based Perovskite Layers for Efficient Solar Cells. *Science* **2017**, *356*, 1376−1379.
(35) Even, J.; Carignano, M.; Katan, C. Molecular Disorder and Translation/Rotation Coupling in the Plastic Crystal Phase of Hybrid Perovskites. *Nanoscale* **2016**, *8*, 6222−6236.
(36) She, L.; Liu, M.; Zhong, D. Atomic Structures of $CH_3NH_3PbI_3$ (001) Surfaces. *ACS Nano* **2016**, *10*, 1126−1131.
(37) Quarti, C.; Mosconi, E.; De Angelis, F. Interplay of Orientational Order and Electronic Structure in Methylammonium Lead Iodide: Implications for Solar Cell Operation. *Chem. Mater.* **2014**, *26*, 6557−6569.
(38) Wyckoff, R. W. G. *Cadmium Chloride Structure*, 2nd ed.; Interscience Publishers: New York, New York, 1963; Vol. *1*, pp 239−444.
(39) Even, J.; Pedesseau, L.; Kepenekian, M. Electronic Surface States and Dielectric Self-Energy Profiles in Colloidal Nanoscale Platelets of CdSe. *Phys. Chem. Chem. Phys.* **2014**, *16*, 25182−25190.
(40) Sapori, D.; Kepenekian, M.; Pedesseau, L.; Katan, C.; Even, J. Quantum Confinement and Dielectric Profiles of Colloidal Nanoplatelets of Halide Inorganic and Hybrid Organic-Inorganic Perovskites. *Nanoscale* **2016**, *8*, 6369−6378.
(41) Gielisse, P. J.; Plendl, J. N.; Mansur, L. C.; Marshall, R.; Mitra, S. S.; Mykolajewycz, R.; Smakula, A. Infrared Properties of NiO and CoO and Their Mixed Crystals. *J. Appl. Phys.* **1965**, *36*, 2446−2450.
(42) Hirasawa, M.; Ishihara, T.; Goto, T.; Uchida, K.; Miura, N. Magnetoabsorption of the Lowest Exciton in Perovskite-Type Compound $(CH_3NH_3)PbI_3$. *Phys. B* **1994**, *201*, 427−430.
(43) Even, J.; Pedesseau, L.; Katan, C. Analysis of Multivalley and Multibandgap Absorption and Enhancement of Free Carriers Related to Exciton Screening in Hybrid Perovskites. *J. Phys. Chem. C* **2014**, *118*, 11566−11572.
(44) Yang, Z.; Surrente, A.; Galkowski, K.; Bruyant, N.; Maude, D. K.; Haghighirad, A. A.; Snaith, H. J.; Plochocka, P.; Nicholas, R. J. Unraveling the Exciton Binding Energy and the Dielectric Constant in Single-Crystal Methylammonium Lead Triiodide Perovskite. *J. Phys. Chem. Lett.* **2017**, *8*, 1851−1855.
(45) Junquera, J.; Zimmer, M.; Ordejón, P.; Ghosez, P. First-principles Calculation of The Band Offset at $BaO/BaTiO_3$ and $SrO/SrTiO_3$ Interfaces. *Phys. Rev. B* **2003**, *67*, No. 155327.
(46) Traore, B.; Pedesseau, L.; Assam, L.; Che, X.; Blancon, J.-C.; Tsai, H.; Nie, W.; Stoumpos, C. C.; Kanatzidis, M. G.; Tretiak, S.; Mohite, A. D.; Even, J.; Kepenekian, M.; Katan, C. Composite Nature of Layered Hybrid Perovskites: Assessment on Quantum and Dielectric Confinements and Band Alignment. *ACS Nano* **2018**, *12*, 3321−3332.
(47) Peressi, M.; Binggeli, N.; Baldereschi, A. Band Engineering at Interfaces: Theory And Numerical Experiments. *J. Phys. D: Appl. Phys.* **1998**, *31*, 1273−1299.
(48) Liu, T.; Chen, K.; Hu, Q.; Zhu, R.; Gong, Q. Inverted Perovskite Solar Cells: Progresses and Perspectives. *Adv. Energy Mater.* **2016**, *6*, No. 1600457.
(49) Niu, G.; Wang, S.; Li, J.; Li, W.; Wang, L. Oxygen Doping in Nickel Oxide For Highly Efficient Planar Perovskite Solar Cells. *J. Mater. Chem. A* **2018**, *6*, 4721−4728.
(50) Heyd, J.; Scuseria, G. E.; Ernzerhof, M. Hybrid Functionals Based on a Screened Coulomb Potential. *J. Chem. Phys.* **2003**, *118*, 8207−8215.
(51) Heyd, J.; Scuseria, G. E.; Ernzerhof, M. Erratum: "Hybrid Functionals Based on a Screened Coulomb Potential". *J. Chem. Phys.* **2003**, *118*, 8207; *J. Chem. Phys.* **2006**, *124*, No. 219906.
(52) Haruyama, J.; Sodeyama, K.; Han, L.; Tateyama, Y. Termination Dependence of Tetragonal $CH_3NH_3PbI_3$ Surfaces for Perovskite Solar Cells. *J. Phys. Chem. Lett.* **2014**, *5*, 2903−2909.
(53) Volonakis, G.; Giustino, F. Interfaces Between Graphene-Related Materials and $MAPbI_3$: Insights from First-Principles. *Adv. Mater. Interfaces* **2018**, *5*, No. 1800496.
(54) Steirer, K. X.; Schulz, P.; Teeter, G.; Stevanovic, V.; Yang, M.; Zhu, K.; Berry, J. J. Defect Tolerance in Methylammonium Lead Triiodide Perovskite. *ACS Energy Lett.* **2016**, *1*, 360−366.
(55) Meggiolaro, D.; De Angelis, F. First-Principles Modeling of Defects in Lead Halide Perovskites: Best Practices and Open Issues. *ACS Energy Lett.* **2018**, *3*, 2206−2222.
(56) Yavari, M.; et al. How Far Does the Defect Tolerance of Lead-Halide Perovskites Range? The Example of Bi Impurities Introducing Efficient Recombination Centers. *J. Mater. Chem. A* **2019**, *7*, 23838−23853.
(57) Meggiolaro, D.; Motti, S. G.; Mosconi, E.; Barker, A. J.; Ball, J.; Andrea Riccardo Perini, C.; Deschler, F.; Petrozza, A.; De Angelis, F. Iodine Chemistry Determines the Defect Tolerance of Lead-Halide Perovskites. *Energy Environ. Sci.* **2018**, *11*, 702−713.
(58) Kim, J.; Lee, S.-H.; Lee, J. H.; Hong, K.-H. The Role of Intrinsic Defects in Methylammonium Lead Iodide Perovskite. *J. Phys. Chem. Lett.* **2014**, *5*, 1312−1317.
(59) Kye, Y.-H.; Yu, C.-J.; Jong, U.-G.; Chen, Y.; Walsh, A. Critical Role of Water in Defect Aggregation and Chemical Degradation of Perovskite Solar Cells. *J. Phys. Chem. Lett.* **2018**, *9*, 2196−2201.
(60) Zhang, W. B.; Yu, N.; Yu, W. Y.; Tang, B. Y. Stability and Magnetism of Vacancy in NiO: A GGA+*U* Study. *Eur. Phys. J. B* **2008**, *64*, 153−158.
(61) Osorio-Guillén, J.; Lany, S.; Zunger, A. Nonstoichiometry and Hole Doping in NiO. *AIP Conf. Proc.* **2010**, *1199*, 128−129.
(62) Jang, W.-L.; Lu, Y.-M.; Hwang, W.-S.; Hsiung, T.-L.; Wang, H. P. Point Defects in Sputtered NiO Films. *Appl. Phys. Lett.* **2009**, *94*, No. 062103.
(63) Kojima, A.; Teshima, K.; Shirai, Y.; Miyasaka, T. Organometal Halide Perovskites as Visible-Light Sensitizers for Photovoltaic Cells. *J. Am. Chem. Soc.* **2009**, *131*, 6050−6051.
(64) Greiner, M. T.; Helander, M. G.; Wang, Z.-B.; Tang, W.-M.; Lu, Z.-H. Effects of Processing Conditions on the Work Function and Energy-Level Alignment of NiO Thin Films. *J. Phys. Chem. C* **2010**, *114*, 19777−19781.
(65) Madjid, A. H.; Martinez, J. M. Thermionic Emission from Nickel Oxide. *Phys. Rev. Lett.* **1972**, *28*, 1313−1315.
(66) Olivier, J.; Servet, B.; Vergnolle, M.; Mosca, M.; Garry, G. Stability/Instability of Conductivity and Work Function Changes of ITO Thin Films, UV-Irradiated in Air or Vacuum: Measurements by the Four-Probe Method and by Kelvin Force Microscopy. *Synth. Met.* **2001**, *122*, 87−89.
(67) Hu, L.; Peng, J.; Wang, W.; Xia, Z.; Yuan, J.; Lu, J.; Huang, X.; Ma, W.; Song, H.; Chen, W.; Cheng, Y.-B.; Tang, J. Sequential Deposition of $CH_3NH_3PbI_3$ on Planar NiO Film for Efficient Planar Perovskite Solar Cells. *ACS Photonics* **2014**, *1*, 547−553.
(68) Zhai, Z.; Huang, X.; Xu, M.; Yuan, J.; Peng, J.; Ma, W. Greatly Reduced Processing Temperature for a Solution-Processed NiO_x Buffer Layer in Polymer Solar Cells. *Adv. Energy Mater.* **2013**, *3*, 1614−1622.
(69) Kamiya, T.; Ohta, H.; Kamiya, M.; Nomura, K.; Ueda, K.; Hirano, M.; Hosono, H. Li-Doped NiO Epitaxial Thin Film with Atomically Flat Surface. *J. Mater. Res.* **2004**, *19*, 913−920.
(70) Jang, W.-L.; Lu, Y.-M.; Hwang, W.-S.; Chen, W.-C. Electrical Properties of Li-Doped NiO Films. *J. Eur. Ceram. Soc.* **2010**, *30*, 503−508.
(71) Park, M.-A.; Park, I. J.; Park, S.; Kim, J.; Jo, W.; Son, H. J.; Kim, J. Y. Enhanced Electrical Properties of Li-Doped NiO_x Hole Extraction Layer in p-i-n Type Perovskite Solar Cells. *Curr. Appl. Phys.* **2018**, *18*, S55−S59.

https://dx.doi.org/10.1021/acsami.9b19457
ACS Appl. Mater. Interfaces 2020, 12, 6633−6640